Published online 29 December 2016 *Nucleic Acids Research, 2017, Vol. 45, No. 6* ***3537–3546***
doi: 10.1093/nar/gkw1307

Structural insights into RNA duplexes with multiple 2′-5′-linkages

Fusheng Shen[1,2,†], Zhipu Luo[3,†], Hehua Liu[4], Rui Wang[1,2], Shenglong Zhang[5], Jianhua Gan[4,*] and Jia Sheng[1,2,*]

[1]Department of Chemistry, University at Albany, State University of New York, Albany, NY 12222, USA, [2]The RNA Institute, University at Albany, State University of New York, Albany, NY 12222, USA, [3]Synchrotron Radiation Research Section, MCL National Cancer Institute, Argonne National Laboratory, Argonne, IL 60439, USA, [4]State Key Laboratory of Genetic Engineering, Collaborative Innovation Center of Genetics and Development, Department of Physiology and Biophysics, School of Life Sciences, Fudan University, Shanghai 200433, China and [5]Department of Life Sciences, New York Institute of Technology, New York, NY 10023, USA

Received November 03, 2016; Revised December 13, 2016; Editorial Decision December 14, 2016; Accepted December 20, 2016

ABSTRACT

2′-5′-linked RNAs play important roles in many biological systems. In addition, the mixture of 2′-5′ and 3′-5′ phosphodiester bonds have emerged as a plausible structural element in prebiotic RNAs. Toward our mechanistic studies of RNA folding and structures with heterogeneous backbones, we recently reported two crystal structures of a decamer RNA duplex containing two and six 2′-5′-linkages, showing how RNA duplexes adjust the structures to accommodate these non-canonical linkages (*Proc. Natl. Acad. Sci. USA*, 2014, 111, 3050–3055). Herein, we present two additional high-resolution crystal structures of the same RNA duplex containing four and eight 2′-5′-linkages at different positions, providing new insights into the effects of these modifications and a dynamic view of RNA structure changes with increased numbers of 2′-5′-linkages in the same duplex. Our results show that the local structural perturbations caused by 2′-5′ linkages can be distributed to nearly all the nucleotides with big ranges of changes in different geometry parameters. In addition, hydration pattern and solvation energy analysis indicate less favorable solvent interactions of 2′-5′-linkages comparing to the native 3′-5′-linkages. This study not only promotes our understanding of RNA backbone flexibility, but also provides a knowledge base for studying the biochemical and prebiotic significance of RNA 2′-5′-linkages.

INTRODUCTION

RNA has been long regarded as the first biopolymer in the original stage of life due to the dual roles it can play as both genetic information carriers and biochemical catalysts (1–4). The template-directed non-enzymatic replication of RNA is a key step toward the evolution of simple cellular life from prebiotic chemistry. (5) In the current model, due to the similar nucleophilicity and orientation of the 2′ and 3′ hydroxyl groups on the ribose, the chemical copying of RNA templates generates a product mixed with both 3′-5′ and 2′-5′ backbone linkages (Figure 1), although the specific formation of native 3′-5′ linkages could be promoted by using different activated monomers or buffers containing various metal ions (6–11). This lack of regiospecificity has been regarded as one of the big problems for the evolution of functional RNAs since the resulting backbone heterogeneity might disrupt the functions of RNA ribozymes such as folding, molecular recognition and catalysis, which are the foundation of the RNA world. However, recent works from Szostak lab have demonstrated the reproducible evolution of functional nucleic acid molecules from the mixture of DNA/RNA backbones, (12) and that the RNA ligand binding and catalytic functions of a flavin mononucleotide binding aptamer and a hammerhead ribozyme is not significantly disrupted by sporadic occurrences of 2′-5′ linkages (13). More interestingly, it has been known for long time that 2′-5′ linkages can reduce the thermal stability of RNA duplexes, facilitating duplex strand separations during the subsequent replication of RNA (13–16). Considering that strand separation is another big issue of non-enzymatic RNA replication (17), the function of lowering the duplex stability actually represents a big evolutionary advantage of 2′-5′-backbone linkages. In addition, previous studies have revealed that 2′-5′ linkages in RNA duplexes

*To whom correspondence should be addressed. Tel: +1 518 437 4419; Fax: +1 518 442 3462; Email: jsheng@albany.edu
Correspondence may also be addressed to Jianhua Gan. Tel/Fax: +86 21 51630543; Email: ganjhh@fudan.edu.cn
† These authors contributed equally to the paper as first authors.

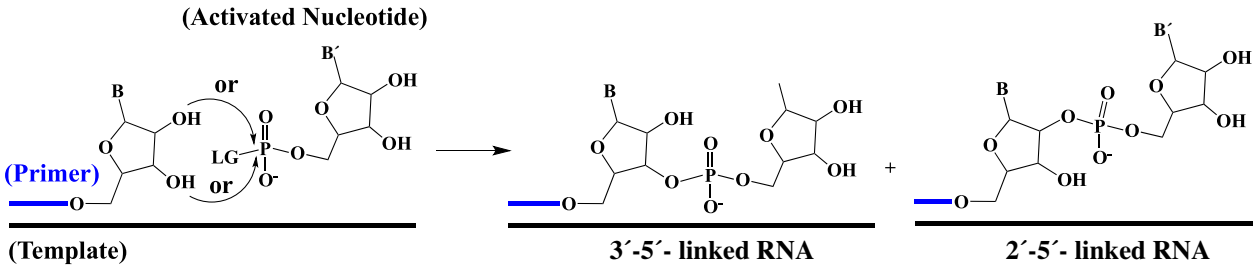

Figure 1. Template-directed chemical incorporation of an activated monomer to a primer. (LG, leaving group, e.g. 2-methylimidazole).

hydrolyze much easier than the normal 3′-5′ linkages (6), resulting in the formation of 2′,3′-cyclic phosphate, which can be selectively converted back to the more stable 3′-5′-linkages under prebiotic conditions (18) and may have been a potential pathway to weeding out most of the 2′-5′ linkages in later stages of RNA world.

These results suggested that the co-existence of 2′-5′ and 3′-5′ backbone linkages may have been one of the essential features of early RNA and play certain roles in the original stage of life, instead of being a problematic issue. More interestingly, probably as relics from the RNA world, 2′-5′ linkages still exist and play critical roles in current biological RNA systems. For example, the Peach Latent Mosaic Viroid, a circular RNA pathogen that can replicate itself in a DNA-independent fashion via a rolling circle mechanism, uses 2′-5′ phosphodiester bonds to circularize its RNA from linear form and to stabilize the circular template for efficient self-replication (19). In human's innate immune response system, the RNA 2′-5′ linkage is used to activate endoribonuclease RNase L and degrade external virus RNAs (20–22). In addition, the 2′-5′ linked oligonucleotides have also been used as antisense therapeutics with improved enzymatic hydrolysis resistance (23–25).

Given the potential importance of 2′-5′-linked RNA in prebiotic and modern biology, we have been working on the structural features and functions of these non-canonical phosphodiester linkages. The study will not only promote our understanding of RNA backbone flexibility, but also provide the knowledge base for studying their biochemical and prebiotic significance, as well as the further optimization of their biomedical applications. Despite the fact that NMR structures of a 2′-5′-DNA:RNA duplex and a few X-ray crystal structures of 2′-5′-linked dinucleotides have been reported (26–34), no crystal structures were available for the 2′-5′/3′-5′ mixed RNA molecules until recently. We have reported the first two high-resolution crystal structures of a self-complementary RNA decamer duplex containing two and six 2′-5′ linkages, respectively (35). These data, along with the following molecular dynamics simulations, provide clear structural insights into the conformation of 2′-5′-linked nucleotides and preliminary information about how RNA duplexes adjust their global and local structures to accommodate these mixed backbones through flexible sugar puckers and the flanking nucleotides compensation effect (35). Herein, we present two additional crystal structures of the same decamer RNA duplex containing four and eight 2′-5′-linkages at different positions. Together with our previously solved structures, this work provides a dynamic view of RNA structure changes with increased numbers of 2′-5′-linkages in the same duplex context. Our results show that the RNA helical structures can be well retained with 40% of backbone heterogeneity. The local structural perturbations caused by 2′-5′ linkages can be distributed to nearly all the nucleotides in the structure with diverse ranges of changes in different geometry parameters. In addition, both hydration pattern and solvation energy analysis suggest that 2′-5′-linkages have less favorable solvent interactions than the native 3′-5′-linkages.

MATERIALS AND METHODS

RNA oligonucleotides preparation

Self-complementary RNA oligonucleotides with CG containing sequence 5′-$(CCGGCGCCGG)_2$-3′ were synthesized by standard solid phase synthesis using Oligo-800 DNA synthesizer. The 3′-TBDMS-2′-CE-phosphoramidites purchased from ChemGenes Corporation were used to synthesize 2′-5′ linked RNA strands 5′-CCG*GC*GCCGG-3′ (referred as 4-25-decamer) and 5′-CCG*GC*GC*CG*G-3′ (referred as 8-25-decamer) with the 2′-5′ linkages denoted by asterisks. Oligonucleotides were deprotected by AMA (1:1 mixture of ammonium hydroxide and methyl amine solution) followed by the $Et_3N{\bullet}3HF$ treatment; and purified by ion-exchange HPLC using Dionex PA-200 column at a flow rate of 1 ml/min with the buffer system containing pure water (buffer A) and 2 M ammonium acetate (pH 7.1, buffer B). The RNA oligonucleotides were eluted with a linear gradient from 0% to 45% buffer B over 20 min. The collected major fractions were lyophilized, desalted and re-concentrated to 1 mM.

Crystallization

RNA samples (0.5 mM duplex) were heated to 80°C for 5 min, slowly cooled down to room temperature (20°C) with the rate of 1°C/min, and placed at 4°C for overnight before crystallization. Nucleic Acid Mini Screen Kits, Natrix (Hampton Research) and Nuc-Pro-HTS (Jena Bioscience) were used to screen crystallization conditions at both 20 and 4°C using the hanging-drop method. Both RNA samples were crystallized by mixing 1 μl of RNA duplex solution with 1 μl of precipitant consisting of 40 mM sodium

cacodylate buffer (pH 7.0), 10% (v/v) MPD (2-methyl-2,4-pentanediol), 12 mM spermine tetrahydrochloride, 40 mM LiCl, 80 mM $SrCl_2$ and 20 mM $MgCl_2$ (No. 22 of the Nucleic Acid Mini Screen kit from Hampton Research) at room temperature in 3–5 days equilibrating with 35% (v/v) MPD as reservoir.

Data collection, structure determination and refinement

Perfluoropolyether was used to soak crystals as the cryoprotectant. The crystals were mounted into the perfluoropolyether drop and kept for 30 s before transferred to liquid nitrogen. Diffraction data were collected at wavelength of 1 Å under a liquid nitrogen stream at −174°C on Beamline 8.2.1 at Advanced Light Source in Lawrence Berkeley National Laboratory (USA). The crystals were exposed for 1 s per image with a 1° of oscillation angle. All the data were processed using HKL2000 (36).

The program PHASER (37) was initially used to solve the crystal structures of both 2′-5′ modified RNAs by molecular replacement using our previously solved 2-25-duplex structure (PDB: 4MSB) as model after removing metal ions and water molecules. One solution was found for 8-25-decamer, however, no solution could be found for the 4-25-decamer. Then MOLREP (38) was carried out using only one chain of our previously solved native structure (PDB: 4MS9) as the search model. Two unpaired asymmetric chains were found. Both structures were refined using Refmac (39). The stereo-chemical topology and geometrical restraint parameters of DNA/RNA were applied (40). To build the 2′-5′ linkage models, the nucleotide whose 2′-OH links to the 5′-phosphorus of the next nucleotide was loaded from monomer library and manually adjusted to fit with the electron density at the modified position in Coot (41). The old unmodified residues in model from molecular replacement were removed, then the 2′-5′ linkages were created by merging the monomers into the truncated model. After several cycles of refinement, a number of highly ordered waters and strontium ions were added. The final models were obtained until the refinement achieves convergence and deposited into PDB data with entry ID 5TDJ for 4-25-decamer and 5TDK for 8-25-decamer. The data collection and refinement statistics of these two structures are listed in Table 1.

Thermal denaturation and CD experiments

Solutions of the duplex RNAs (0.5 μM) were prepared by dissolving the purified oligonucleotides in 10 mM sodium phosphate (pH 6.5) with 100 mM NaCl. The solutions were heated to 90°C for 3 min, then cooled slowly to room temperature, and stored at 4°C for overnight. Thermal denaturation was performed in a Cary 300 UV-Visible Spectrophotometer equipped with a temperature controller. The temperature reported is the block temperature. Each curve was acquired at 260 nm by heating and cooling from 5 to 85°C four times at a rate of 0.5°C/min. Experiments were repeated for four times. CD studies were carried out in the same buffer utilizing a Jasco-815 CD spectrometer at room temperature in a quartz cell with a 10-mm path length. CD spectra were collected from 380 to 200 nm and with a scanning speed of 100 nm/min. The bandwidth was 1.0 nm, and the digital integration time was 1.0 s. All CD spectra were baseline-corrected for signal contributions due to the buffer.

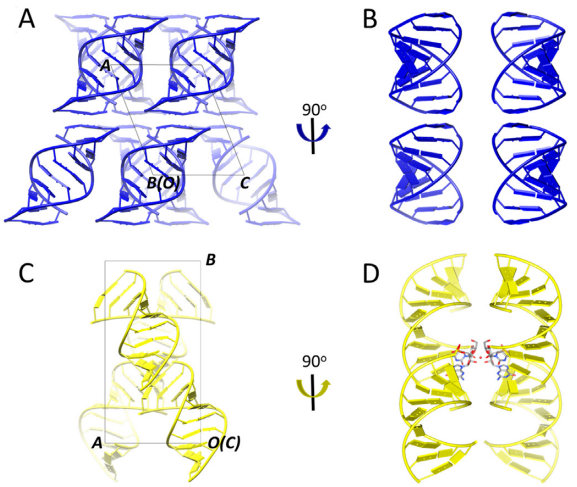

Figure 2. Crystal packing of (**A** and **B**) 4-25-decamer and (**C** and **D**) 8-25-decamer RNA duplexes. RNA duplexes are shown as cartoon with all bases demonstrated as slab except four bases (shown as stick) close to a water molecule (red sphere) located on a 2-fold axis in (**D**).

RESULTS

Molecular packing and overall helical interactions

Both of the modified RNA duplexes crystallized in the space group of *C*2. There is one paired duplex in the asymmetric unit of 8-25-decamer crystal, while in the asymmetric unit of 4-25-decamer, there are two separated single strands, which form duplexes with their symmetry mates. To determine whether the 2′-5′-linked residues are directly involved in the molecular packing, we investigated the helix–helix interactions in each crystal lattice. Each paired duplex of 4-25-decamer generated by symmetry operation elongate along the two helical axes of the two asymmetric duplexes. One of the helical axis is parallel to the short diagonal of face *ac*, and the other parallel to cell edge *a* (Figure 2A). The terminal base pairs of consecutive duplexes along helical axes are stacked together (Figure 2A and B). Each adjacent duplexes parallel to the helical axes are linked together through the formation of several hydrogen bonds involving backbones and sugars (Supplementary Figure S1A). The 8–25 RNA duplex extends along the helical axes parallel to each diagonal of face *ab* at an angle of 55.7° (Figure 2C). Similar to the 4–25 pattern, the consecutive helices stack on each other in a head-to-tail fashion with the 3′-terminal G10:C1 pair of one helix staked on the C1:G10 pair of another helix, forming continuous helical chains. Notably, the two terminal guanosine bases are very close to each other at each helical junction with the distance between the two O6 atoms only 2.8 Å (Supplementary Figure S1C). More interestingly, a water molecule at 2-fold axis of the unit cell forms perfect hydrogen bonds within four adjacent duplexes (Figure 2D and Supplementary Figure S1B). One duplex can interact with another two parallel neighboring duplexes through hydrogen bonds (Supplementary Figure S1D). Similar as our previous solved 2–25 and 6–25 structures, the O3′ atoms of

Table 1. The statistics of X-ray data collection and structure refinement of the RNA decamer duplexes with four and eight 2′-5′-linkages

	4-25-decamer (PDB ID: 5TDJ)	8-25-decamer (PDB ID:5TDK)
Scaling		
Space group	*C* 2	*C* 2
Unit cell parameters, Å	27.5 × 94.5 × 21.3	24.8 × 47.0 × 42.9
Unit cell parameters, degrees	90, 111.2, 90	90.0, 96.5, 90.0
Resolution range, Å (last shell)	30–1.50 (1.55–1.50)	18.69–1.43 (1.47–1.43)
Unique reflections (last shell)	7870 (721)	8980 (632)
Completeness, %	96.7 (88.7)	98.6 (91.9)
R_{merge},%	6.4 (55.4)	6.3 (67.8)
$<I/\sigma(I)>$	18.3 (1.8)	13.3 (2.0)
Redundancy	3.9 (3.0)	5.2 (6.3)
Refinement		
Resolution range, Å	19.90–1.50	18.69–1.43
Number of reflections	7093	8504
Completeness, %	96.7	98.5
R_{work}, %	15.2	16.8
R_{free}, %	17.0	20.6
Bond length rmsd, Å	0.0099	0.0104
Bond angle rmsd, degrees	1.96	1.38
Overall B-factor with water, Å^2	33.7	19.0

bases at the 2′-5′-linked steps are directly involved in the duplex–duplex interactions, as shown in the three zoom-in views of Supplementary Figure S1A and Supplementary Figure S1B.

Overall helical structures of multiple 2′-5′ linked RNAs

As expected, both of these two multiple 2′-5′-linked RNA strands form A-type duplexes. The superimposed comparison with our previously solved two structures containing two (referred as 2-25-decamer) and six (referred as 6-25-decamer) 2′-5′-linkages in the same sequence context (all the sequences are shown in Figure 3A) shows very similar overall duplex structures (Figure 3B) with slight winding of each helical axis that is connecting the centroid of each base pair (Figure 3C). These 2′-5′-linked RNAs also have very high structural isomorphism to their native counterpart with the overall root mean square deviations (r.m.s.d.) are 1.22, 0.55, 1.70 and 1.38 Å for two, four, six and eight 2′-5′-linked decamers, respectively. Figure 3D shows the alignment of the backbones that connect each phosphorus atoms in the same strand. Obvious compressed or 'kinked' backbones have been observed in the previous 2-25-decamer and 6-25-decamer structures with the distances between two terminal phosphorus atoms (P2-P10) being 22.9 Å and 21.8 Å, respectively, comparing to 25.4 Å in native duplex. However, in the 4-25-decamer strands, the distance of P2-P10 (25.3 Å) is almost identical to the one in native duplex, while in the 8-25-decamer structure, the distance is 21.8 Å, identical to the one in the 6-25-decamer structure. This comparison indicates that the addition of 2′-5′ linkages is not directly correlated with the strand compressing. While the locations of 2′-5′ linkages might have more effects on the overall duplex conformation, the relatively small r.m.s.d values of duplexes and big distance range of P2-P10 with different numbers of 2′-5′ linkages confirm that the RNA duplex structures are quite flexible and can be dynamically adjusted to accommodate backbone heterogeneity without causing dramatic global changes.

Helical parameters and overall duplex Flexibility with Multiple 2′-5′ linkages

To further compare these RNA structures with more quantitative details, we calculated their local base-pair, base pair helical and step parameters using 3DNA (43). Consistent with the duplex superimpose view, the average values of each geometric parameters are very similar within all the five structures (Supplementary Tables S1 and S2). Within the local base pair parameters, stagger and propeller show most obvious changes with the different numbers of 2′-5′ linkages. In the stagger pattern (Figure 4A), comparing to the native structure (represented by the green up-triangle line), the introduction of single 2′-5′ linkage at C5 position in each strand (red diamond line) causes significant increase of stagger distance especially in G4, C5 and G6 pairs. The additional 2′-5′ linkage at G3 (blue cycle line) further increase the stagger of C5 and G6 pairs, while decreasing the one in G4 pair. The further introduction of 2′-5′ linkages at C7 (cyan square line) and G9 (dark yellow down-triangle line) positions, however, decreases the stagger of both C5 and G6 pairs gradually back to the native level. Instead, the stagger distances of G3, G9 and G10 pairs are dramatically increased for about 0.4 Å and stagger into opposite directions with the two additional 2′-5′ linkages. The propeller pattern (Figure 4B) shows that the introduction of 2′-5′ linkages decreases the overall propeller angles for up to 10°. Particularly, the G4 pair propels to opposite direction with over 20° changes (from −15° to 5°) in the 6–25 structure (cyan line), while switching back to −5° with an additional 2′-5′ linkage in the G9 position, which is far away from the G4 pair. While all these changes are cascade effects of each connected base pairs and it is difficult to attribute them to a particular single 2′-5′ linkage, the 2′-5′ linked base pairs seem to have better flexibility and buffering capacity comparing to the native ones.

It has been shown from our previous structural analysis that the x-displacement, slide and rise are the three base pair step parameters that have most obvious changes induced by the 2′-5′ linkages. The introduction of one 2′-5′ linkage at each C5 residue increases ∼2 Å of x-displacement (red line

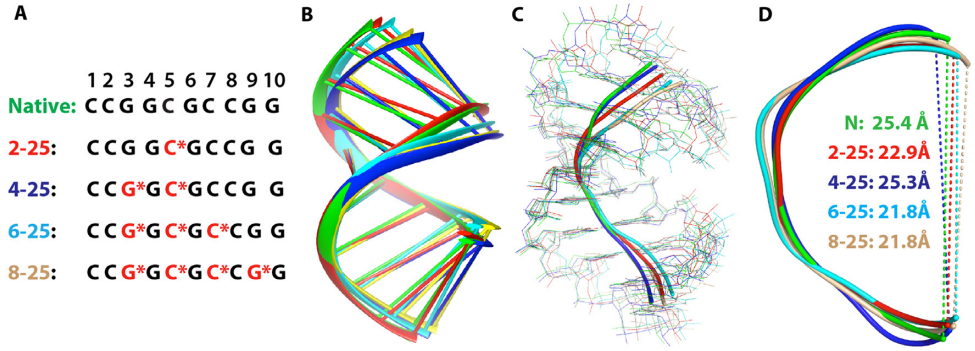

Figure 3. (**A**) Sequences of the native and 2′-5′-linked RNA decamers with 2′-5′-linked residues labeled as red asterisks. (**B**) The superimposed duplex comparison of native (green), 2–25 (red), 4–25 (blue), 6–25 (cyan) and 8–25 (dark yellow). (**C**) Duplex comparison shown with the winding axis connecting the centroids of each base pair. (**D**) The backbone distances measured between P1 and P9 in each duplex (backbone coordinates are generated by program CURVES (42)).

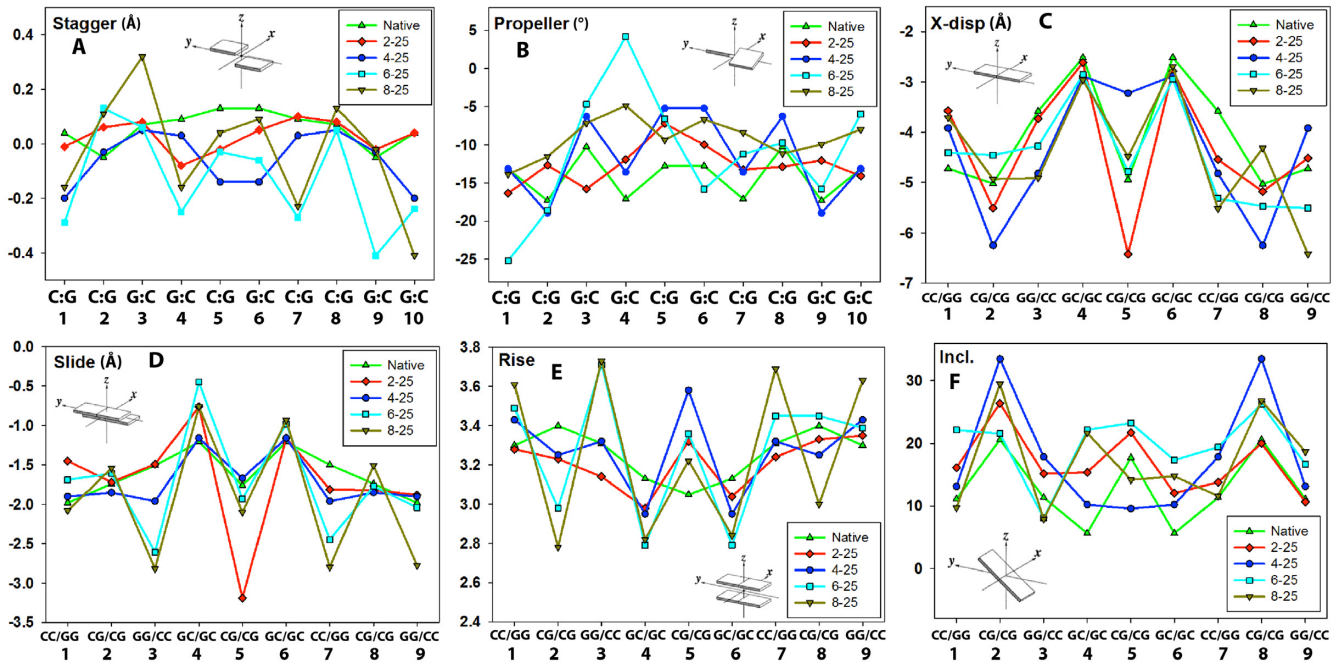

Figure 4. Local base pair and base-pair step parameters. (**A**) Stagger, (**B**) Propeller, (**C**) X-displacement, (**D**) Slide, (**E**) Rise (Å) and (**F**) Inclination (°) of native and the four 2′-5′ linked RNA decamers.

versus green line in Figure 4C) for the C5-G6 step. While the 2nd 2′-5′ linkage at G3 position decreases this C5 x-displacement for ∼3.5 Å (red line versus blue line), it further increases this parameter at other positions except the G4-C5 and G6-C7, where all the x-displacements of these five structures are interestingly very similar to each other. The further addition of 2′-5′ linkages stretches the x-disp of C5-G6 step back to the native level while causing obviously fluctuation at the two terminal C2-G3 and C8-G9 steps. Similarly, the slide at C5-G6 step shows the largest increase (∼1.6 Å) in the 2–25 duplex (Figure 4D, red line) and gradually decrease to the native distance with more 2′-5′ linkages in each strands. Meanwhile, the slides at G3-G4 and C7-C8 step gradually increase for ∼1.4 Å when there are more 2′-5′ linkages present and the slides at C2-G3 and C8-G9 steps in all the 2′-5′ structures remain very similar as native one. The rise of each base pair steps drops for ∼0.1–0.2 Å except the C5-G6 step in the 2-25-decamer structure (Figure 4E, red line versus green line). The same trend is observed in 4–25 structure (blue line) where the rise of C5-G6 reaches to 3.6 Å, (almost 0.5 Å higher than native one), and the rises of G3-G4 and C7-C8 restore to the native one. One additional 2′-5′ linkage in 6–25 structure (cyan line) decreases the rise of all the three middle steps including G4-C5, C5-G6 and G6-C7, as well as the C2-G3; but dramatically increase the rise level between G3-G4 to 3.7 Å, which is 0.4 Å higher than native and 2–25 ones. In the 8–25 structure (dark yellow line), all the rise in each base step distribute equally centering on the native values with a big range from 2.8 to 3.7 Å. Another base pair step helical parameter that has similar trend is inclination (Figure 4F). The introduction of first 2′-5′ linkage between C5-G6 (red line) increases most of the

inclination angles. The 2nd 2′-5′ linkage (blue line) further increase the angles at C2-G3 and C8-G9 to the maximum (∼15° over the native one) while decreasing the middle C5-G6 step for over 10°. The 3rd 2′-5′ linkage between C7-C8 (cyan line), however, increases most of the inclination values while decreasing the ones at C2-G3 and C8-G9 steps.

Helical groove widths

We further measured the groove widths of these five duplexes to study the impact of 2′-5′-linkages to the overall helix structures. The direct distances between the cross-stranded phosphate atoms (44) were analyzed as shown in Figure 5 and Supplementary Table S3. Similar as each individual structural geometry, the widths of both major and minor grooves fluctuate with increased numbers of 2′-5′-linkages. The introduction of single 2′-5′-linkage compresses the major groove and open the minor groove for ∼0.5 Å in the central region of the duplex (the red versus green lines in Figure 5A and B). The second 2′-5′-linkage, instead, opens the major groove for ∼1 Å except in the central C5 position, while retaining almost the same minor groove size as the native one (blue versus green lines). Introducing the next two 2′-5′-linkages further expands the major groove in the G3, G6 and C7 positions for maximum 2 Å and compress it in the G4 and C5 positions for ∼1 Å (Figure 5A, cyan and dark yellow lines). Accordingly, the minor groove widths (Figure 5B, cyan and dark yellow lines) decrease in the G3, G6 and C7 positions but fluctuate in both G4 and C5 positions. Overall, the 2′-5′-linkages in the duplex can dynamically either open or compress both major and minor grooves in different positions with minimal change in the middle of duplex (C5 position). The maximum change of major groove width locates in the G6 position; and the two terminal positions have the maximum change of minor groove widths.

Sugar pucker conformations of 2′-5′-linked nucleotides

The flexible sugar pucker conformation of 2′-5′-linked nucleosides might be one of the major players to adjust the local structures and accommodate different extent of backbone heterogeneity with diverse structural geometries in the duplex context. It has been reported from previous NMR studies that the 2′-5′-linked nucleosides take 2′-endo sugar pucker conformation, which results in longer distances between its 5′- and 2′- phosphorous atoms than the normal 3′-5′-linked one (45,46). We also observed all the 2′-endo, 3′-endo and the mixed forms of sugar puckers in our previously solved 2′-5′-RNA duplexes with the formation of a potential hydrogen bond between the free 3′-OH and one of the oxygen atom in the 2′-phosphate group (35). Consistently, in the two new duplex structures with four and eight 2′-5′-linkages, most of the 2′-5′-nucleotides take the 2′-endo sugar pucker except the G9 in the 3′-end of the 8–25 structure (Supplementary Table S4). Each 2′-5′-linked base step has quite flexible local geometries with different distances between 3′-OH and phosphate oxygen atom ranging from 3.0 Å (Figure 6C) to 4.1 Å (Figure 6B), and between the two 1′-carbon atoms ranging from 5.5 Å (Figure 6B) to 6.5 Å (Figure 6A). With the 2′-endo sugar pucker, the 2′-5′-linked G-G step has obvious shorter C1′-C1′ distance than the C-G and C-C steps (Figure 6B). The switching of sugar pucker to 3′-endo (e.g. G9 in the 8–25 structure, Figure 6D) expands the distance between the two guanine bases but decreases the distance between 3′-OH and phosphate oxygen comparing to the similar G-G step in Figure 6B, resulting in further bending of the phosphate backbone at this site. It has been demonstrated that the energy difference between the two sugar puckers are relatively small (35,47) and they can dynamically switch to each other. The various distances observed in these base steps further confirm the dynamic vibration of these 2′-5′-linked residues.

It has been known that the 2′-5′-linked RNA duplexes are easier to be hydrolyzed than the normal 3′-5′-linked ones (6,9) and our previous structural work showed that the O3′-P-O5′ angles in the 2′-5′ linked base steps are much bigger than the O2′-P-O5′ angles in the 3′-5′ linked residues, positioning the O3′ atom closer to an ‘in-line’ conformation with P-O5′ bond (35). Consistently, we observed the ‘in-line’ mode of O3′-P-O5′ in all the 2′-5′ linked nucleotides with slightly different angles. Taking the base steps in Figure 6 as examples, the O3′-P-O5′ angles in 2′-5′ linked C-G, G-G and C-C with 2′-endo sugar pucker are 116.9°, 120.4° and 107.9°, respectively (Supplementary Figure S2A–C). Interestingly, in the G-G step with 3′-endo sugar pucker, the angle is 159.4° (Supplementary Figure S2D), placing the O3′ atom even closer to a completely linear alignment with P-O5′ bond. These residues might also be the most labile positions in the 2′-5′ linked RNA strands during the hydrolysis. In comparison, both C-G and G-G steps with native 3′-5′ linkages take much smaller angles as ∼70° (Supplementary Figure S2E and F).

Hydration and solvation energy of 2′-5′-linked RNA duplexes

Our native RNA structure (PDB: 4MS9) shows that almost every 2′-OH group on the ribose has interactions with several highly conserved water molecules in the minor groove. In comparison, the 3′-OH groups in the 2′-5′-linkages have much less hydrogen bonding interactions with surrounding water molecules. We only observed three 2′-5′-linked nucleotides that are involved in the water interactions including the G3-G4 and C7-C8 steps in the 6–25 structure (Figure 7A and B), where one water molecule bridges the 3′-OH and one of the phosphate oxygen, as well as the G3-G4 step in 8–25 structure (Figure 7C), where two water molecules are involved in the hydrogen bonds with the 3′-OH. Interestingly, none of the middle 2′-5′-linked C4-G5 step in all the four duplexes contains any water interaction. The less participation of the 3′-OH in hydration networks is also consistent with the higher structural flexibility of the 2′-5′-linked nucleotides. On the other hand, the nucleobases in the 2′-5′-linked nucleotides are usually highly involved in the hydration networks with highly conserved water molecules and the phosphate oxygen atoms. One typical pattern is shown in Figure 7D, where three highly conserved water molecules connect the 2′-5′-linked C5-G6 step with the C7 residue through the hydrogen bonding with the nucleobases. These interactions might contribute to the pre-

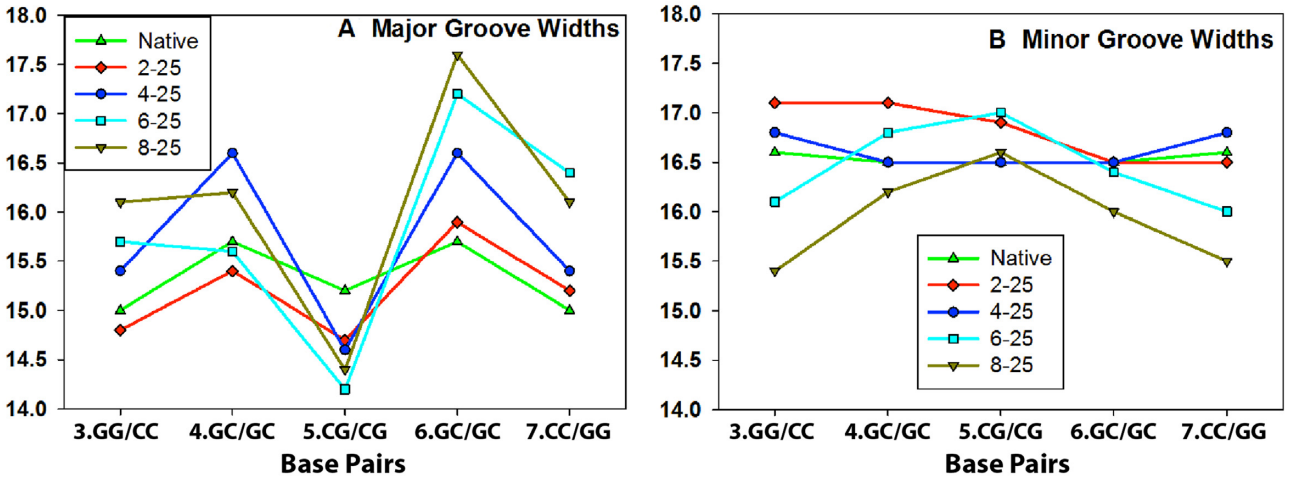

Figure 5. The effects of 2′-5′-linkages to the over helical structures in (**A**) major groove widths (Å); and (**B**) minor groove widths (Å) in different base pair steps. The groove widths are measured by the direct P-P distances cross the strands (P_i-P_{i+2}).

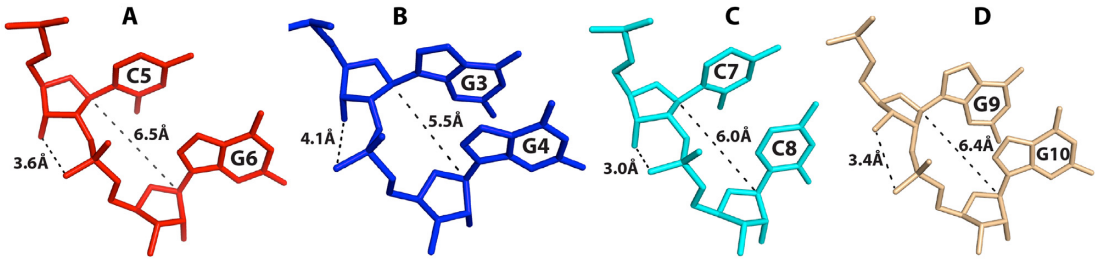

Figure 6. 2′-5′-linked base steps in the four modified structures labeled with the distances between the two 1′ carbon atoms, and between the 3′-OH and its closest oxygen atom of phosphate on next residual. (**A**) C5-G6 step in 2–25 structure; (**B**) G3-G4 step in 4–25 structure; (**C**) C7-C8 step in 6–25 structure; and (**D**) G9-G10 in 8–25 structure with the G9 taking 3′-endo sugar pucker. The color codes are consistent with the previous figures.

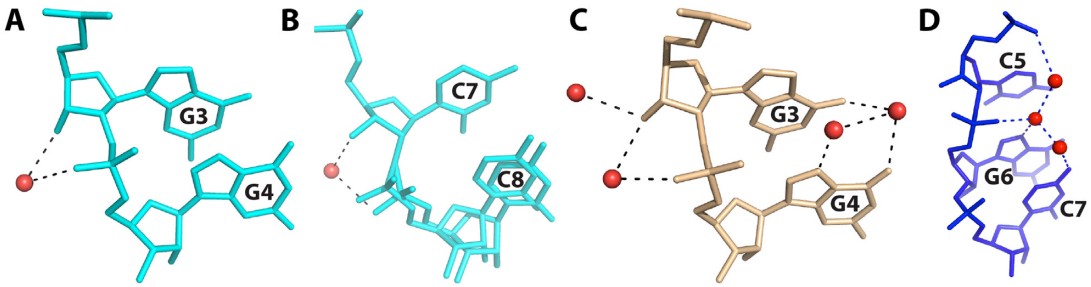

Figure 7. The water mediated hydrogen bonding interactions involved in the 2′-5′-linked base steps. (**A**) G3-G4 step in 6–25 structure; (**B**) C7-C8 step in 6–25 structure with two flexible conformations of C8; (**C**) G3-G4 step in 8–25 structure; and (**D**) C5-G6-C7 steps in 4–25 structure. The red spheres represent the highly conserved water molecules; and the color codes are consistent with the previous figures.

organization of each single RNA strands for the formation of duplex structures.

The solvation energies of each 2′-5′-linked and native RNA duplexes were subsequently calculated using the 'solvate' module of the SEQMOL program. As shown in Supplementary Table S5, the introduction of the first two 2′-5′-linkages significantly decreases the solvation energies of the two duplexes with approximately 60 $Å^2$ less accessible surface area than the native one. However, the additional 2′-5′-linkages in 6–25 structure result in bigger accessible surface areas than native one for 68 $Å^2$; and the accessible surface area is further increased for 70 $Å^2$ in the 8–25 structure. This big range of total accessible surface areas observed in the 2′-5′-linked RNA duplexes are also consistent with the above-described diverse structural geometries. On the other hand, the solvation energies of both 6–25 and 8–25 duplexes are slightly decreased in comparison with the native one.

DISCUSSION

One of the original aims of this work is to generalize the correlation between the structural changes and the introduction of each 2′-5′-linkages at different positions and different base steps. Overall, since each geometric parameter has been affecting each other and they have integrated contribu-

tions to both local and global structural changes of the duplexes, it seems to be very complicated and difficult to generalize these rules. Nevertheless, the systematic comparison of these geometric parameters indicates the strong cooperative effects of multiple 2′-5′-linkages in the same duplex to accommodate or buffer most of the structural changes. The local perturbations caused by the 2′-5′-linkages could be distributed not only to the flanking bases but also to the remote residues far away from the linkages, showing the overall structural flexibility of RNA duplexes with backbone heterogeneity. In addition, these structural analyses show the 2′-5′-linked nucleotides are prone to change their geometries much easier than the native 3′-5′-linked ones in responding to the additional 2′-5′-linkages. We have made an animation for a more direct view of the dynamic structural changes of these RNA duplexes with increased numbers of 2′-5′-linkages, as shown in the additional online Supporting Data.

One important characteristic feature of 2′-5′-linked RNA duplexes is their decreased thermal stability comparing to the native counterparts. For a RNA duplex, the more 2′-5′-linkages, the lower the thermal stability is (13–16). In addition, it has been known from the previous study that the increased numbers of 2′-5′-linkages decrease the overall RNA duplex stability in a linear fashion, and that the destabilization effect is also dependent on the 2′-5′-linked residues, the positions as well as the arrangement of these 2′-5′-linkages within the duplex (14). In the current GC-10mer sequence context, as shown in Table 2 and Supplementary Figure S3, the incorporation of the first two 2′-5′-linkages dramatically decreases the duplex T_m for ∼9°C, while the 4–25 duplex retains very similar T_m with the 2–25 one, and the T_m of 6–25 and 8–25 duplex with extra two and four 2′-5′-linkages only decrease for ∼7°C. These data indicate that the 2′-5′-linkages reduce the overall duplex thermal stability in a cooperative way, which can be attributed to the relatively big ranges of structural flexibility and the resulted maximum duplex formation. It has been proposed that the perturbation of base step rise plays dominating roles in destabilizing these 2′-5′-linked duplexes (43,48). This is also consistent with the large fluctuations rise values we observed in Figure 4E, which are quite far away from the optimal 3.3 Å (49) and result in the diminished base stacking interactions. In addition to the rise values, the overlap areas between each base pair steps might also affect the overall stacking interactions. As shown in Supplementary Table S6, the total overlap area including both intra-strand and inter-strand overlapping of the four 2′-5′-RNA duplexes are 54.29, 51.90, 51.04 and 50.01 Å^2, respectively, similar to the total area of 53.54 Å^2 in the native duplex. Interestingly, the total overlap area of 2–25 duplex is even higher than the native one despite a ∼9°C of T_m drop, indicating that the difference of duplex overlapping areas caused by the 2′-5′-linkages might not be significant to lower the stability of RNA duplex.

Although the absolute energy calculation from the theoretical molecular simulation is not accurate, the lower solvation energies associated with the larger duplex accessible surface areas of the 2′-5′-linked RNA indicates that the 2′-5′-linkages have less favorable solvent interactions comparing to the native 3′-5′-linkages, which is also consistent with our observation that there are much fewer highly ordered water molecules interacting with the 2′-5′-backbone. Since hydration can directly affect the overall duplex stability (50), the energy difference we observed here might be another contributing factor to adjust the thermal stability of 2′-5′-linked RNA duplexes.

To study their overall conformation in solution, we further measured the circular dichroism spectra of 2′-5′-linked RNA duplexes. As shown in Supplementary Figure S4, all the duplexes show characteristic peaks of the A-form helical conformation with a strong positive peak around 270 nm and a weak negative peak around 240 nm (51,52). Comparing to the native duplex, 2′-5′-linked ones have slight upshifts on the positive peak and show a relatively strong negative peak at ∼210 nm. Consistent with the duplex comparison, these CD spectra also confirm the high structural isomorphism of 2′-5′-linked duplexes with subtle local changes in solution. It is known that comparing to normal 3′-5′-linkages, the 2′-5′-linked backbones are more 'pushed' into the minor groove, which is characterized as wide and shallow in A-form duplexes (33,53). As a result, the minor groove can better accommodate the backbone heterogeneity with its width changes relatively smaller than the major groove. The non-regular helical structures might also facilitate the dissociation of these RNA duplexes at certain positions and enable them to functionalize as 'aptamers', which diversify the functions of early RNAs through binding with other environmental components including small molecule ligands, metal ions and other RNA species toward the evolution of more complicated RNA machineries with specific functions. On the other hand, the variable major groove widths caused by the 2′-5′-linkages might play important roles in the enzymatic recognition of 2′-5′-linked RNA duplexes in currently biological systems. For example, the RNA:2′-5′-RNA duplexes are known to be able to bind the enzyme RNase H as the non-active substrates (15).

CONCLUSION

In this work, we present two new high-resolution crystal structures of RNA-decamer duplexes containing four and eight 2′-5′ backbone linkages. The systematic structural comparison with our two previously-solved structures containing two and six 2′-5′ linkages within the same sequence context, together with the native counterpart, provides a dynamic view of how RNA duplex switches its structure with increased numbers of 2′-5′ linkages. Our results show that the RNA helical structures have striking duplex plasticity and can be well retained with even 40% of 2′-5′ backbone heterogeneity. The local structural perturbations caused by 2′-5′ linkages can be accommodated and distributed to nearly all the nucleotides in the structure with diverse ranges of changes in several different geometry parameters. The detailed geometric analysis of the current four crystal structures indicates that each structural parameters could fluctuate in a big range and the 2′-5′-linked nucleotides are relatively easy to change their geometries comparing to the native 3′-5′-linked ones in responding to the additional 2′-5′ incorporations. Since the 2′-5′ linkages are primarily located in the wide minor groove of A-form RNA duplex, they are observed to widen the duplex major grooves more than minor grooves. In addition, both hydration pattern and energy

Table 2. Melting temperatures of native and each 2′-5′-linked RNA duplexes

RNA duplex	T_m (°C)[a]	ΔT_m (°C)[b]
Native	74.1	—
2–25	65.5	−8.6
4–25	63.1	−11
6–25	59.2	−14.9
8–25	58.2	−15.9

[a] T_ms were measured in 10 mM sodium phosphate (pH 7.0) containing 100 mM NaCl. T_m values are the averages of four measurements.
[b] ΔT_m values are relative to the native duplex.

analysis suggest that 2′-5′-linkages have less favorable solvent interactions in comparison to the native 3′-5′-linkages, which might also contribute to the lower thermal stability of 2′-5′-linked RNA duplexes. Overall, these dynamic structural changes and the associated lower RNA duplex stability caused by the 2′-5′ linkages might have represented the evolutionary significance that enables these hybrid RNAs to develop more diversified functions and interactions with other environmental components toward the evolution of more complicated RNA machineries. However, more systematic RNA structures containing different distribution patterns of 2′-5′-linkages in more sequence contexts are still required in order to find out the general rules correlating the detailed structural changes with the additions of each 2′-5′ linkages at different positions. These studies will also promote our better understanding of the current biological functions of RNA 2′-5′ linkages and contribute to the rational design of 2′-5′-linked RNAs as antisense strands in their biomedical applications.

AVAILABILITY

Detailed base-pair, base-pair step and base-pair helical parameters, base pair overlap area, duplex groove widths, sugar pucker conformation, the solvation energy, the UV-melting and CD curves of the 2′-5′-linked RNA duplexes. The two new RNA structures have been deposited in Protein Data Bank (www.rcsb.org) with the PDB IDs: 5TDJ (4-25-duplex) and 5TDK (8-25-duplex).

SUPPLEMENTARY DATA

Supplementary Data are available at NAR Online.

ACKNOWLEDGEMENTS

The authors thank Chun Pong Tam, Dr. Aaron Engelhart and Dr. Katarzyna Adamala for the helpful discussion and Dr. Wen Zhang for the help in data collection. All the X-ray diffraction data were collected at the Advanced Light Source (ALS) beamlines 8.2.1 and 8.2.2. The Berkeley Center for Structural Biology is supported in part by the National Institutes of Health, National Institute of General Medical Sciences, and the Howard Hughes Medical Institute. The Advanced Light Source is supported by the Director, Office of Science, Office of Basic Energy Sciences, of the U.S. Department of Energy under Contract No. DE-AC02-05CH11231.

FUNDING

University at Albany, State University of New York; postdoctoral fellowship from Simons Foundation [338863 to R.W.]; Key Research and Development Project of China [2016YFA0500600 to J.G.]; National Natural Science Foundation of China [31370728 to J.G.]. Funding for open access charge: University at Albany; State University of New York.
Conflict of interest statement. None declared.

REFERENCES

1. Crick,F.H. (1968) The origin of the genetic code. *J. Mol. Biol.*, **38**, 367–379.
2. Gilbert,W. (1986) The RNA world. *Nature*, **319**, 618.
3. Joyce,G.F. (1989) RNA evolution and the origins of life. *Nature*, **338**, 217–224.
4. Orgel,L.E. (1968) Evolution of the genetic apparatus. *J. Mol. Biol.*, **38**, 381–393.
5. Mansy,S.S., Schrum,J.P., Krishnamurthy,M., Tobe,S., Treco,D.A. and Szostak,J.W. (2008) Template-directed synthesis of a genetic polymer in a model protocell. *Nature*, **454**, 122–125.
6. Usher,D.A. and McHale,A.H. (1976) Hydrolytic stability of helical RNA: a selective advantage for the natural 3′,5′-bond. *Proc. Natl. Acad. Sci. U.S.A.*, **73**, 1149–1153.
7. Bridson,P.K. and Orgel,L.E. (1980) Catalysis of accurate poly(C)-directed synthesis of 3′-5′-linked oligoguanylates by Zn^{2+}. *J. Mol. Biol.*, **144**, 567–577.
8. Inoue,T. and Orgel,L.E. (1982) Oligomerization of (guanosine 5′-phosphor)-2-methylimidazolide on poly(C). An RNA polymerase model. *J. Mol. Biol.*, **162**, 201–217.
9. Rohatgi,R., Bartel,D.P. and Szostak,J.W. (1996) Nonenzymatic, template-directed ligation of oligoribonucleotides is highly regioselective for the formation of 3′-5′ phosphodiester bonds. *J. Am. Chem. Soc.*, **118**, 3340–3344.
10. Ekland,E.H. and Bartel,D.P. (1996) RNA-catalysed RNA polymerization using nucleoside triphosphates. *Nature*, **382**, 373–376.
11. Johnston,W.K., Unrau,P.J., Lawrence,M.S., Glasner,M.E. and Bartel,D.P. (2001) RNA-catalyzed RNA polymerization: accurate and general RNA-templated primer extension. *Science*, **292**, 1319–1325.
12. Trevino,S.G., Zhang,N., Elenko,M.P., Luptak,A. and Szostak,J.W. (2011) Evolution of functional nucleic acids in the presence of nonheritable backbone heterogeneity. *Proc. Natl. Acad. Sci. U.S.A.*, **108**, 13492–13497.
13. Engelhart,A.E., Powner,M.W. and Szostak,J.W. (2013) Functional RNAs exhibit tolerance for non-heritable 2′-5′ versus 3′-5′ backbone heterogeneity. *Nat. Chem.*, **5**, 390–394.
14. Giannaris,P.A. and Damha,M.J. (1993) Oligoribonucleotides containing 2′,5′-phosphodiester linkages exhibit binding selectivity for 3′,5′-RNA over 3′,5′-ssDNA. *Nucleic Acids Res.*, **21**, 4742–4749.
15. Wasner,M., Arion,D., Borkow,G., Noronha,A., Uddin,A.H., Parniak,M.A. and Damha,M.J. (1998) Physicochemical and biochemical properties of 2′,5′-linked RNA and 2′,5′-RNA:3′,5′-RNA "hybrid" duplexes. *Biochemistry*, **37**, 7478–7486.
16. Kierzek,R., He,L. and Turner,D.H. (1992) Association of 2′-5′ oligoribonucleotides. *Nucleic Acids Res.*, **20**, 1685–1690.
17. Szostak,J.W. (2012) The eightfold path to non-enzymatic RNA replication. *J. Syst. Chem.*, **3**, 2–14.

18. Bowler,F.R., Chan,C.K., Duffy,C.D., Gerland,B., Islam,S., Powner,M.W., Sutherland,J.D. and Xu,J. (2013) Prebiotically plausible oligoribonucleotide ligation facilitated by chemoselective acetylation. *Nat. Chem.*, **5**, 383–389.
19. Cote,F., Levesque,D. and Perreault,J.P. (2001) Natural 2′,5′-phosphodiester bonds found at the ligation sites of peach latent mosaic viroid. *J. Virol.*, **75**, 19–25.
20. Hovanessian,A.G. and Justesen,J. (2007) The human 2′-5′oligoadenylate synthetase family: unique interferon-inducible enzymes catalyzing 2′-5′ instead of 3′-5′ phosphodiester bond formation. *Biochimie*, **89**, 779–788.
21. Player,M.R. and Torrence,P.F. (1998) The 2-5A system: modulation of viral and cellular processes through acceleration of RNA degradation. *Pharmacol. Ther.*, **78**, 55–113.
22. Wreschner,D.H., James,T.C., Silverman,R.H. and Kerr,I.M. (1981) Ribosomal RNA cleavage, nuclease activation and 2-5A(ppp(A2′p)nA) in interferon-treated cells. *Nucleic Acids Res.*, **9**, 1571–1581.
23. Bhan,P., Bhan,A., Hong,M., Hartwell,J.G., Saunders,J.M. and Hoke,G.D. (1997) 2′,5′-linked oligo-3′-deoxyribonucleoside phosphorothioate chimeras: thermal stability and antisense inhibition of gene expression. *Nucleic Acids Res.*, **25**, 3310–3317.
24. Kandimalla,E.R., Manning,A., Zhao,Q., Shaw,D.R., Byrn,R.A., Sasisekharan,V. and Agrawal,S. (1997) Mixed backbone antisense oligonucleotides: design, biochemical and biological properties of oligonucleotides containing 2′-5′-ribo- and 3′-5′-deoxyribonucleotide segments. *Nucleic Acids Res.*, **25**, 370–378.
25. Xiao,W., Li,G., Maitra,R.K., Maran,A., Silverman,R.H. and Torrence,P.F. (1997) Correlation of selective modifications to a 2′,5′-oligoadenylate-3′,5′-deoxyribonucleotide antisense chimera with affinity for the target nucleic acid and with ability to activate RNase L. *J. Med. Chem.*, **40**, 1195–1200.
26. Horowitz,E.D., Lilavivat,S., Holladay,B.W., Germann,M.W. and Hud,N.V. (2009) Solution structure and thermodynamics of 2′,5′ RNA intercalation. *J. Am. Chem. Soc.*, **131**, 5831–5838.
27. Premraj,B.J., Raja,S., Bhavesh,N.S., Shi,K., Hosur,R.V., Sundaralingam,M. and Yathindra,N. (2004) Solution structure of 2′,5′ d(G4C4). Relevance to topological restrictions and nature's choice of phosphodiester links. *Eur. J. Biochem.*, **271**, 2956–2966.
28. Plevnik,M., Gdaniec,Z. and Plavec,J. (2005) Solution structure of a modified 2′,5′-linked RNA hairpin involved in an equilibrium with duplex. *Nucleic Acids Res.*, **33**, 1749–1759.
29. Premraj,B.J., Patel,P.K., Kandimalla,E.R., Agrawal,S., Hosur,R.V. and Yathindra,N. (2001) NMR structure of a 2′,5′ RNA favors A type duplex with compact C2′endo nucleotide repeat. *Biochem. Biophys. Res. Commun.*, **283**, 537–543.
30. Krishnan,R., Seshadri,T.P. and Viswamitra,M.A. (1991) Visualisation of a 2′-5′ parallel stranded double helix at atomic resolution: crystal structure of cytidylyl-2′,5′-adenosine. *Nucleic Acids Res.*, **19**, 379–384.
31. Dhingra,M.M. and Sarma,R.H. (1978) Why do nucleic acids have 3′5′ phosphodiester bonds? *Nature*, **272**, 798–801.
32. Parthasarathy,R., Malik,M. and Fridey,S.M. (1982) X-ray structure of a dinucleoside monophosphate A2′p5′C that contains a 2′-5′ link found in (2′-5′)oligo(A)s induced by interferons: single-stranded helical conformation of 2′-5′-linked oligonucleotides. *Proc. Natl. Acad. Sci. U.S.A.*, **79**, 7292–7296.
33. Robinson,H., Jung,K.-E., Switzer,C. and Wang,A.H.J. (1995) DNA with 2′-5′ Phosphodiester Bonds Forms a Duplex Structure in the A-type Conformation. *J. Am. Chem. Soc.*, **117**, 837–838.
34. Premraj,B.J., Raja,S. and Yathindra,N. (2002) Structural basis for the unusual properties of 2′,5′ nucleic acids and their complexes with RNA and DNA. *Biophys. Chem.*, **95**, 253–272.
35. Sheng,J., Li,L., Engelhart,A.E., Gan,J., Wang,J. and Szostak,J.W. (2014) Structural insights into the effects of 2′-5′ linkages on the RNA duplex. *Proc. Natl. Acad. Sci. U.S.A.*, **111**, 3050–3055.
36. Otwinowski,Z. and Minor,W. (1997) Processing of X-ray Diffraction Data Collected in Oscillation Mode. *Methods Enzymol.*, **276**, 307–326.
37. McCoy,A.J., Grosse-Kunstleve,R.W., Adams,P.D., Winn,M.D., Storoni,L.C. and Read,R.J. (2007) Phaser crystallographic software. *J. Appl. Crystallogr.*, **40**, 658–674.
38. Vagin,A. and Teplyakov,A. (1997) MOLREP: an Automated Program for Molecular Replacement. *J. Appl. Cryst.*, **30**, 1022–1025.
39. Murshudov,G.N., Vagin,A.A. and Dodson,E.J. (1997) Refinement of macromolecular structures by the maximum-likelihood method. *Acta Crystallogr. D Biol. Crystallogr.*, **53**, 240–255.
40. Parkinson,G., Vojtechovsky,J., Clowney,L., Brunger,A.T. and Berman,H.M. (1996) New parameters for the refinement of nucleic acid-containing structures. *Acta Crystallogr. D Biol. Crystallogr.*, **52**, 57–64.
41. Emsley,P. and Cowtan,K. (2004) Coot: model-building tools for molecular graphics. *Acta Crystallogr. D Biol. Crystallogr.*, **60**, 2126–2132.
42. Lavery,R., Moakher,M., Maddocks,J.H., Petkeviciute,D. and Zakrzewska,K. (2009) Conformational analysis of nucleic acids revisited: Curves+. *Nucleic Acids Res.*, **37**, 5917–5929.
43. Lu,X.J. and Olson,W.K. (2008) 3DNA: a versatile, integrated software system for the analysis, rebuilding and visualization of three-dimensional nucleic-acid structures. *Nat. Protoc.*, **3**, 1213–1227.
44. El Hassan,M.A. and Calladine,C.R. (1998) Two distinct modes of protein-induced bending in DNA. *J. Mol. Biol.*, **282**, 331–343.
45. Salazar,M., Champoux,J.J. and Reid,B.R. (1993) Sugar conformations at hybrid duplex junctions in HIV-1 and Okazaki fragments. *Biochemistry*, **32**, 739–744.
46. Salazar,M., Fedoroff,O.Y. and Reid,B.R. (1996) Structure of chimeric duplex junctions: solution conformation of the retroviral Okazaki-like fragment r(ccca)d(AATGA).d(TCATTTGGG) from Moloney murine leukemia virus. *Biochemistry*, **35**, 8126–8135.
47. Li,L. and Szostak,J.W. (2014) The free energy landscape of pseudorotation in 3′-5′ and 2′-5′ linked nucleic acids. *J. Am. Chem. Soc.*, **136**, 2858–2865.
48. Dickerson,R.E. (1989) Definitions and nomenclature of nucleic acid structure components. *Nucleic Acids Res.*, **17**, 1797–1803.
49. Parker,T.M., Hohenstein,E.G., Parrish,R.M., Hud,N.V. and Sherrill,C.D. (2013) Quantum-mechanical analysis of the energetic contributions to π; stacking in nucleic acids versus rise, twist, and slide. *J. Am. Chem. Soc.*, **135**, 1306–1316.
50. Barsky,D., Colvin,M.E., Zon,G. and Gryaznov,S.M. (1997) Hydration effects on the duplex stability of phosphoramidate DNA-RNA oligomers. *Nucleic Acids Res.*, **25**, 830–835.
51. Hall,K.B. and McLaughlin,L.W. (1991) Thermodynamic and structural properties of pentamer DNA.DNA, RNA.RNA, and DNA.RNA duplexes of identical sequence. *Biochemistry*, **30**, 10606–10613.
52. Ratmeyer,L., Vinayak,R., Zhong,Y.Y., Zon,G. and Wilson,W.D. (1994) Sequence specific thermodynamic and structural properties for DNA.RNA duplexes. *Biochemistry*, **33**, 5298–5304.
53. Pudlo,J.S., Cao,X., Swaminathan,S. and Matteucci,M.D. (1994) Deoxyoligonucleotides containing 2′,5′ acetal linkages: Synthesis and hybridization properties. *Tetrahedron Lett.*, **35**, 9315–9318.